

**THE EFFECT OF MICROGRAVITY DIRECTION  
ON  
THE GROWTH OF PbSnTe**

**A.L. Fripp, and W.J. Debnam  
NASA, Langley Research Center  
Hampton, VA 23681**

**Phone: 757-864-1503  
FAX: 757-864-7891  
email: a.l.fripp@larc.nasa.gov**

**W.R. Rosch  
National Research Council  
Langley Research Center**

**R. Narayanan  
Chemical Engineering  
University of Florida, Gainesville, FL 32611**

**Introduction**

**The Space Shuttle, Columbia, was launched as STS-75 at 2018 GMT on February 22, 1996. One of the two major experiment packages was the third United States Microgravity Payload (USMP-3), and one of the principal instruments on the USMP was the Advanced Automated Directional Solidification Furnace (AADSf). The AADSf is a multizone directional solidification furnace, and at the time of the USMP-3 flight, capable of processing only one sample per Shuttle mission which, for that flight, was a lead tin telluride (PbSnTe) crystal growth experiment. Archibald L. Fripp, of The Langley Research Center, was the Principal Investigator.**

**In the one year since the flight experiment the sample has been retrieved from the spacecraft and analysis has begun. After presenting introductory material on why PbSnTe was chosen as a test material, why microgravity processing was expected to produce desired results, and what we expected to find in conducting these tests, this report will discuss the results to date which are far from complete.**

## Lead Tin Telluride:

Lead tin telluride is an alloy of PbTe and SnTe. The technological importance of PbSnTe lies in its band gap versus composition diagram which has a zero energy crossing at approximately 40% SnTe. This facilitates the construction of long wavelength ( $>6 \mu\text{m}$ ) infrared detectors and lasers. The properties and utilization of PbSnTe are the subject of other papers.<sup>1,2</sup>

PbSnTe is amenable to study because it is easily compounded, it has a relatively low vapor pressure, and it is miscible with the same crystal structure for all compositions. There is also existing, though limited, literature on its growth and properties. The nominal composition for this work is 20% SnTe and 80% PbTe that produces a bandgap to match the long wavelength atmospheric window.

PbSnTe is also interesting from a purely scientific point of view. It is, potentially, both solutally and thermally unstable due to the temperature and density gradients present during growth. Density gradients, through thermal expansion, are imposed in directional solidification because temperature gradients are required to extract heat. Solutal gradients occur in directional solidification of alloys due to segregation at the interface. The gradients vary with both experiment design and inherent materials properties.

In a simplified one dimensional analysis with the growth axis parallel to the gravity vector only one of the two instabilities works at a time. During growth, the temperature in the liquid increases ahead of the interface. Therefore the density, due to thermal expansion, is decreasing in that direction. However, the phase diagram shows that the lighter SnTe is preferentially rejected at the interface. This causes the liquid density to increase with distance away from the interface which is opposite from the density change due to the furnace temperature profile. Figure 1 is a plot of the composition vs axial position a typical Earth grown crystal. The data points are plotted along with the analytical solution for the totally mixed case.

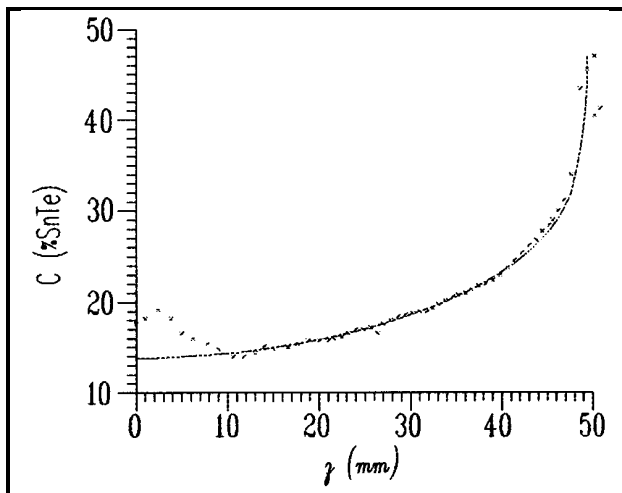


**Figure 1**

Axial composition of Earth grown PbSnTe crystal. The solid line is from the analytical equation for totally mixed melt. This crystal was grown in a low gradient furnace, hence the first to freeze region is larger than that of crystals grown in the AADSF.

Coriell et al.<sup>3</sup> have shown that the two opposing density gradients cannot be readily balanced to stabilize the flow. Moreover, both experiments<sup>4,5,6,7</sup> and numerical analyses<sup>5,8</sup> have demonstrated that radial thermal gradients will start fluid motion long before the onset of convection predicted by a one dimensional model. Hence, there will always be convection in the liquid.

Computational fluid dynamics was utilized to predict the extent of convection in microgravity. The CFD calculations were based on a finite volume technique<sup>9</sup>. The computational code allowed the calculations of time dependent three dimensional flows and associated temperature and concentration profiles. The method behind the calculations involves the division of the calculation domain into a number of cells and then the field equations for mass, momentum and energy conservation are integrated over the volume of the cell. The calculation routine then involves the prediction of the field variables of temperature, concentration, velocity components and pressure at the various cell faces.

In practice, the finite volume technique is used iteratively. Temperature and concentration fields are first guessed; they affect the body force through their effect on buoyancy. The corresponding velocity and pressure fields are then calculated. The computed velocity field is used to correct the earlier estimate of the temperature and solutal concentration field and the process continues until a desired convergence is reached.

This procedure is best explained by considering figure 2. The ampoule liquid region is assumed to be constant as the solidification rates are normally very small. The boundary conditions indicate hot and cold zones as well as insulating zones. The far field concentration is assumed to be constant and the interface condition respects mass conservation along with solutal segregation. The effect of the magnitude of the gravity vector is seen in figures 3 and 4, and we immediately conclude that the flow at low frequency low amplitude accelerations ( $10^{-5} g_e$ ) will be of a

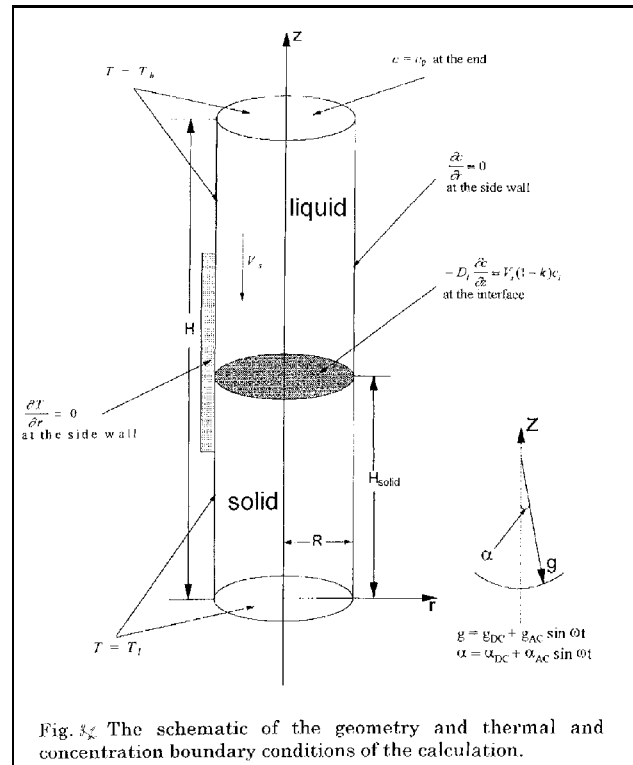


**Figure 2**  
Schematic of the geometric, thermal, and concentration boundary conditions used in the computational fluid dynamical calculations in this study.

weak toroid. Higher amplitude forces will cause solutal convection to come into play, but such high amplitude acceleration vectors were not present at the low frequency levels during USMP-3 and were mainly associated with high frequency activities such as booster firings and water dumps. While we do not presently have any predictions on the effects of high frequency g-jitter it is clear from the order of magnitude of the calculated velocity vectors for the case of low frequency with  $10^{-5}g_e$  that very little mixing should take place. The velocity is no greater than  $10^{-5}$  cm/ sec. Given an initial liquid region size of 5 cm, this small velocity amounts to an initial mixing time of  $10^6$  seconds. Meanwhile the solidification is at the rate of 1 cm/ hour. When the liquid region size is about 1 cm the mixing time is about  $2 \times 10^5$  seconds. Clearly this is insignificant because the entire growth period is about  $2 \times 10^4$  seconds. In other words we predict that only diffusion controlled growth ought to prevail at  $10^{-5}g_e$  and this is even more true at the lower gravitational levels experienced during the USMP-3 mission.

The effect of a five degree offset with respect to the vertical orientation was calculated and the results are graphically shown in figure 3 (c). What is seen from this figure is that small tilts give rise to swirling flow and this flow contains the solutal boundary layer to the depleting surface. This

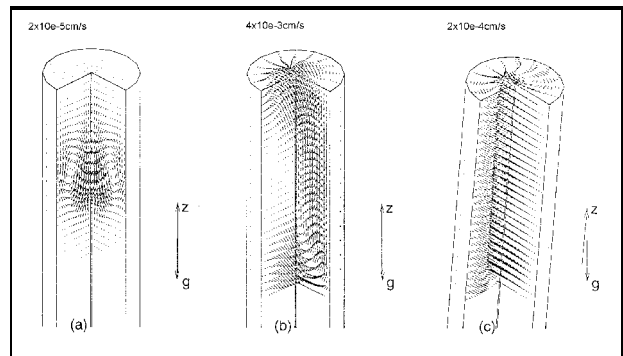


**Figure 4**  
The three dimensional flow field in the liquid region with constant acceleration magnitude and direction. (a) Acceleration is aligned with ampoule axis at  $10^{-5}$  Earth gravity. (b) Acceleration is aligned with ampoule axis at  $10^{-4}$  Earth gravity. (c) Acceleration is misaligned with ampoule axis by  $5^\circ$  with magnitude of  $10^{-5}$  Earth gravity.

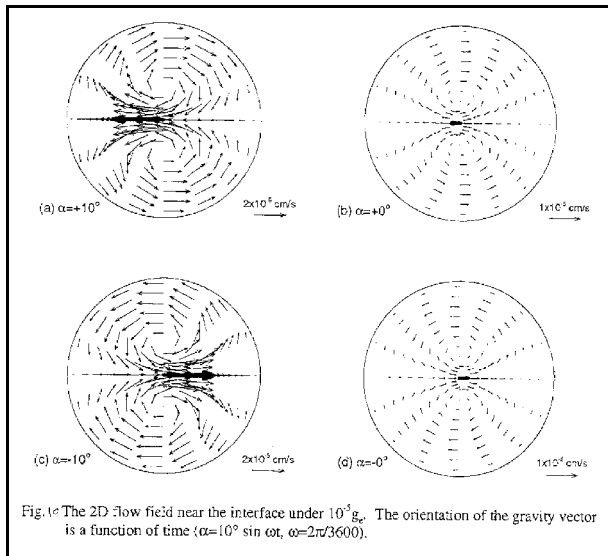


**Figure 3**  
The two dimensional flow field near the melt solid interface when the acceleration vector (magnitude of  $10^{-5}$  Earth gravity) is undergoing a  $10^\circ$  time dependent tilt variation at a frequency of one cycle per hour.

may be contrasted with toroidal flow in figure 3 (a) ( for the vertical orientation) that sweeps the solute out of the solutal boundary layer. The solutal boundary layer contains most of the rejected SnTe and so swirling flow if anything should help by making diffusive growth more probable. In other words one might conclude that a constant off axis arrangement is better than if the acceleration vector were perfectly aligned along the ampoule.

Figure 4 is a depiction of the mixing patterns that are seen when the ampoule is subjected to a time dependent tilt. It must be noted that the velocities are still very small and so even in the case when the tilt is a periodic function of time the growth is expected to be diffusion controlled.

In summary we have concluded that diffusive growth was predicted under low frequency g-jitter conditions. The high frequency was not studied but we did conclude that the time constant for the fastest transporting mechanism (heat transfer) was much larger than the corresponding period for high frequency ( 5 Hz) g-jitter.

### Bridgman Growth:

Bridgman crystal growth offers the opportunity to independently fix the temperature gradient and interface position with respect to the furnace. However, these parameters cannot be varied without bound. There are temperature limits on the furnace and ampoule as well as limits imposed by the growth process. An excellent review of recent advances in Bridgman growth has been given by Favier.<sup>10</sup>

The limits imposed by the growth process are primarily concerned with maintaining an initial solutal translation zone of reasonable length and preventing interfacial instability. Second order problems are the maintenance of interface shape control, and thermal strain in the solid.

Due to the size of the AADSF, a sufficiently high growth rate is required to achieve steady state composition within 20 to 30 millimeters of the start of growth. The furnace must then be controlled to produce an axial thermal gradient in the melt that is sufficient to maintain a stable interface. If the growth is diffusion controlled, the growth distance needed to get within 1% of compositional steady state, i.e. uniform, growth is<sup>11</sup>

$$z_{ss} = 5D/kR . \quad (1)$$

However, the permissible growth rate is limited by the fundamental phenomena of interface breakdown. The short form of the equation for preventing breakdown is

$$\frac{G_T}{R} > \frac{C_s (1-k)}{D k} |m|. \quad (2)$$

Equation one shows that a short initial transition zone requires a high growth rate while equation two shows that a high growth rate requires a large thermal gradient to avoid interfacial breakdown. Increasing either the axial thermal gradient or the growth rate increases the density gradient and the mixing in the liquid. Consequently, it can be seen that there is a trade off between growth rate, temperature gradient and the degree of mixing for a given acceleration level.

The PbSnTe growth experiment on USMP-3 was launched in February 1996. During the flight, three separate crystals were grown in a single, segmented ampoule. The crystals were grown in series, each in one of the three primary orientations with respect to the residual acceleration vector. The growths were roughly analogous to hot-on-top, cold-on-top, and horizontal growth.

While the immediate objective of that experiment was to grow PbSnTe and establish its fundamental growth properties, another, more important objective was to gain a better understanding of the mechanisms involved in generalized crystal growth, particularly those affected by gravity. This information will not only help produce better quality materials on Earth, but also help define future efforts of crystal growth in space and lead the way to more extensive materials science research.

### Segmented Ampoule:

As mentioned before, the USMP-3 AADSF experiment used a single segmented ampoule to grow three separate PbSnTe crystals in series. The ampoule, represented in figure 5, allows each of the three crystals to grow with different conditions without affecting the outcome of the others. For USMP-3, each crystal was grown identically except for the orientation of the ampoule with respect to the residual acceleration<sup>12</sup> vector.

Even though the use of a three cell ampoule decreases the total crystal length, and the percentage of crystal grown where the growth rate nearly matches the translation rate it allows each of the cells to be grown under nearly identical conditions. A long crystal will obtain a nearly thermal steady state growth region sandwiched between two end effect thermal and compositional transient regions. Using the three cell sample decreases the length of any steady state region, however, it provides growth conditions that are nearly thermally equivalent for each of the three cells. Most important, it keeps the composition for the three different regions separated, so that each crystal will have identical starting compositions. Each cell is long enough to reach compositional steady state before the liquid diffusion tail reaches the end of the ampoule.

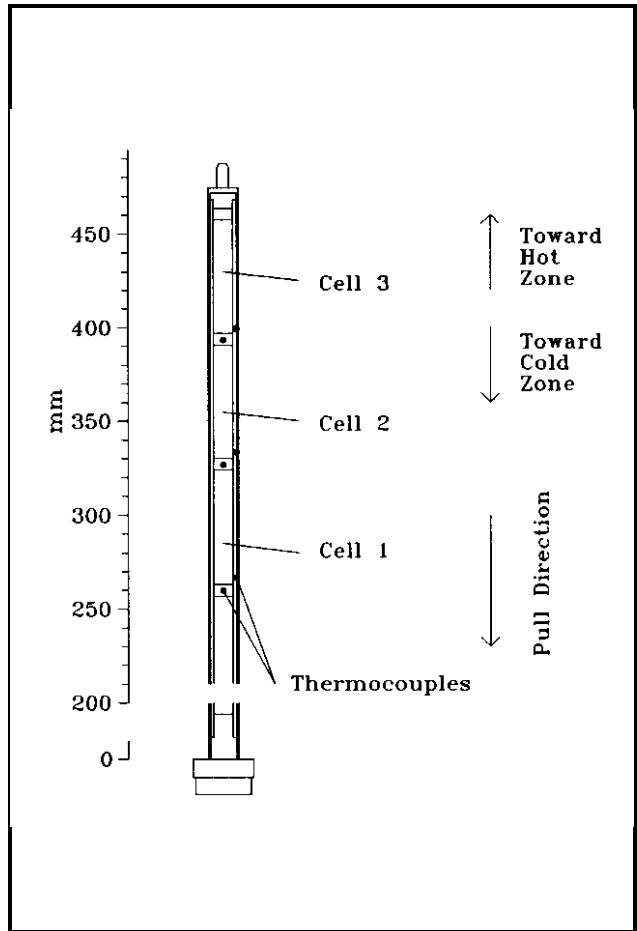


**Figure 5**  
A typical segmented ampoule showing the three cells, and the location of the sample thermocouples.

## Results

### Flight Operations

The Space Shuttle, Columbia, was launched as STS-75 at 2018 GMT on February 22, 1996. The launch time defined Mission Elapse Time (MET) 0 days/ 00 hours: 00 minutes. This nomenclature, MET x/yy:zz, without units, will be used to identify the relative time of events through the text.

With the sample withdrawn 35 mm (ampoule positions will be given by a translation position measurement, tpm, taken as the distance the ampoule is extracted, in mm, from full insertion, hence the present position is tpm = 35) from its fully inserted launch position, the AADSF started heating at MET 06/10:07. The furnace was at temperature, hot zone 1150 °C and cold zone 525 °C, at MET 06/14. After a four hour thermal stabilization period the sample was repositioned to tpm = 37 where tc 1, in the base of cell #1, read 930 °C, which was the so called 'start condition'.

Translation, at 10 mm/hr, to nucleate a seed in cell #1 started at MET 06/20:50. As deep undercooling<sup>13</sup> is not anticipated

and the recalescence event is clearly obvious, at least on Earth, nucleation was expected within 15 cm (1 hr 30 min) after the start of translation. As of MET 06/22:55 no recalescence had been noted, and the translation was reversed to remelt, assuming nucleation had occurred, the solidified portion of the sample and reexamine the small temperature rise in tc 1 observed at 06/21:55. The sample was taken back to tpm = 37 and extraction translation resumed at MET 07/03:14, and the same perturbation in tc 1 occurred approximately 1 hr 5 min into the translation as it had done so the first time around (see figure 6). This was taken as confirmation of recalescence and translation was stopped at MET 07/04:23. This remelting and re-nucleation procedure did not leave sufficient time for solutal diffusion before our 'microgravity time' ended for day seven. An extra day for AADSF operations was requested and received.

At 08/02:14 the Shuttle was put into attitude pitch = 184.5°, yaw = 0°, and roll = 7° which had been calculated<sup>12</sup> to produce a nominal hot on top growth with respect to the microgravity acceleration vector. Dedicated microgravity time for cell #1 began at MET 08/03:00, and translation to grow the crystal in cell #1 started one hour later.

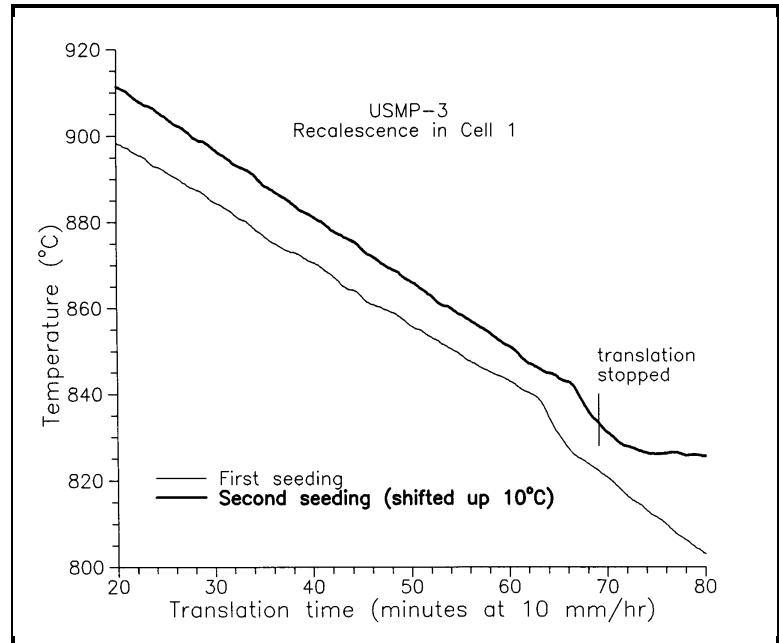


**Figure 6**

Temperature response the recalescence in cell #1. The response did not show a sharp peak as in Earth grown events, but showed a rounded temperature change. The event was repeated (upper curve displaced by 10 °C for clarity) to verify the observation.

At MET 08/06:11, approximately 20 mm into the crystal growth, the Shuttle was put into an unscheduled free drift to help warm up a cold thruster nozzle. During a loss of signal (LOS) period the drift extended past expectations and at 08/06:41 had reached pitch = 187.6°, yaw = 5.2°, and roll = 27.9°. The Shuttle attitude was back to nominal settings by MET 08/06:48, but during the free drift time the acceleration vector alignment with respect to the furnace axis went from approximately 2° to approximately 45°. Figure 7 shows the three axis acceleration measurements, at the AADSF position, during this period.

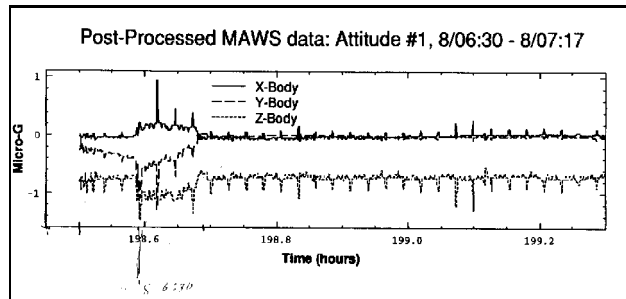


**Figure 7**

The acceleration magnitudes, at the AADSF freeze zone, for each of the three primary directions. The Z acceleration is along the AADSF furnace bore and in such direction that more dense fluid would move from the hot zone toward the cold zone. This time slice shows the acceleration during the free drift period that occurred at approximately MET 8/06:30 (198.6 hours on the graph).

Translation was to continue until recalescence in cell #2. Both thermocouples in cell #2 were inoperable by this time so this step had to depend on knowledge of prior furnace calibration and tpm position rather than the observation of recalescence temperature changes. Translation continued to tpm = 120 which is well past the anticipated recalescence position and then reversed to tpm = 114.75 to remelt excess seed material. At this time all furnace translation stopped until the next dedicated microgravity time.

The Shuttle was positioned in attitude; pitch = 90°, yaw = -17°, and roll = 0° at MET 09/02:19. Microgravity time began at MET 09/03:00, and translation commenced one hour later to grow the crystal in cell #2. The cell #2 growth proceeded without any observed perturbations however the anticipated advent of recalescence in cell #3 looked as if it would occur in the midst of a forthcoming LOS period starting at approximately MET 9/11:12. As described previously, the plan had been to pause the furnace before the LOS, wait until re-acquisition of signal, and then continue translation. However the diminution of the recalescence signal received from space as compared to that observed on Earth made reading the event amongst the stopping and starting of ampoule translation unlikely. It was decided to maintain the translation during the LOS, continue looking for the recalescence after the LOS until such tpm position where translation would have been stopped if both thermocouples had failed as with cell #2, and then to patch in the delayed transmission temperature data onto the curve as soon as it was available.

Translation was stopped at MET 9/11:36. The playback of LOS temperature data came in at 9/11:56 and showed that the recalescence in cell #3 occurred at about 9/11:17, the middle of the LOS. The translation was reversed for 2.5 mm to remelt part of the seed and then was stopped at tpm = 184.7 at MET 9/13:49 to await the next microgravity period to grow the crystal in cell #3.

The Shuttle went into the prescribed attitude; pitch = 123°, yaw = 0°, and roll = 0°; at MET 10/02:03. Microgravity time started at 10/03:00, and translation started at 10/04:00. The sample processed without major incident, and translation ceased at MET 10/10:36:48 at tpm = 250.28. A controlled furnace cool down started at MET 10/11:40:55. The ampoule was stored in the cold furnace at MET 10/20:02.

### Acceleration Magnitudes and Directions

Calculation of the acceleration vectors at the insulation zone of the AADSF as a function of the Space Shuttle attitude produces a transcendental equation as the resultant transformation matrix is dependent on time and attitude varying drag, orbit shape and altitude, and the distance and direction of the AADSF from the center of gravity of the Shuttle. See references <sup>14,15,16</sup>, and <sup>17</sup> for more information on this topic. As the attitude to produce what is essentially hot on top, hot on bottom, and horizontal growths could not be obtained from minimization of the transformation equation a study<sup>18</sup> was undertaken to try to zero in on the preferred attitudes. This and a subsequent, unpublished, study determined the Shuttle attitudes for the three different growth orientations with the following acceleration vectors and concomitant angles.

Note: The following values are nominal. They vary with, among other things, Shuttle drift, orbit position, and sun angle. Also, directions are given in body coordinates for the direction an object would travel in a less massive fluid. In this system an object, at the AADSF location, in attitude #1 would travel away from the center of the Shuttle through the cargo bay doors. This direction is from the hot zone of the AADSF toward the cold zone which is analogous to hot on top furnace orientation on Earth.

Attitude #1, Hot on top growth.

Pitch = 185°, Yaw = 0°, Roll = 7°

Acceleration along the Z axis = -0.75 micro g

Acceleration along the X axis = 0.01 micro g

Acceleration along the Y axis = 0.02 micro g

Approximate angle of acceleration vector with respect to AADSF center bore is

approximately 2°. The desired angle is 0°.

**Attitude #2, Hot on top bottom.**

**Pitch = 90°, Yaw = -17°, Roll = 0°**

**Acceleration along the Z axis = 0.2 to 0.4 micro g**

**Acceleration along the X axis = -0.01 micro g**

**Acceleration along the Y axis = 0.1 micro g**

**Approximate angle of acceleration vector with respect to AADSF center bore is 140° to 160°. The desired angle is 180°.**

**Attitude # 3, Horizontal growth.**

**Pitch = 123°, Yaw = 0°, Roll = 0°**

**Acceleration along the Z axis = 0.1 to 0.1 micro g**

**Acceleration along the X axis = -0.4 micro g**

**Acceleration along the Y axis = 0.15 micro g**

**Approximate angle of acceleration vector with respect to AADSF center bore is -76° to 76°. The desired angle is 90°.**

None of these attitudes are ideal. The attitude #1 is closest to that desired, and attitude #3 averages to the desired value of 90°, but the 14° variation is not desirable.

In addition to the drag and position effects of the low frequency accelerations on the sample the drag deceleration and the tendency for the orbiter to get into an aerodynamically stable mode necessitated the need for vernier booster firings. The forces associated with these corrective measures were of high magnitude (roughly  $10^{-3}g_e$  -  $10^{-4}g_e$ ) but were of a high frequency ( 5-10 Hz).

Comparison of these calculations to the measurements made in flight will be the subject of a subsequent paper.

### Results, Post Flight:

#### X and Gamma Ray Radiography

The flight sample was retrieved from the AADSF at the Kennedy Space Center in April 1996. Microfocus x-ray was used to examine the quartz ampoule for cracks before removal of the Inconel cartridge. No cracks in the fused quartz ampoule

were observed, but the shadow outline of the crystals appeared much longer than expected.

The samples were further examined, still in the Inconel cartridge, with the 420 KV computer aided tomography (CAT) unit also available in the KSC non-destructive test laboratory. These high voltage x-rays are capable of penetrating the PbSnTe samples and exposing any voids, large pits, and bubbles. The results shown by this examination were totally unexpected; the crystals are cratered with large voids and riddled with meandering channels. Figure 8 shows a selected vertical slice of each crystal. This figure was made by reconstructing the transverse slices gathered in the normal CAT fashion. The CAT slices of each crystal are shown in figures 9 to 11.

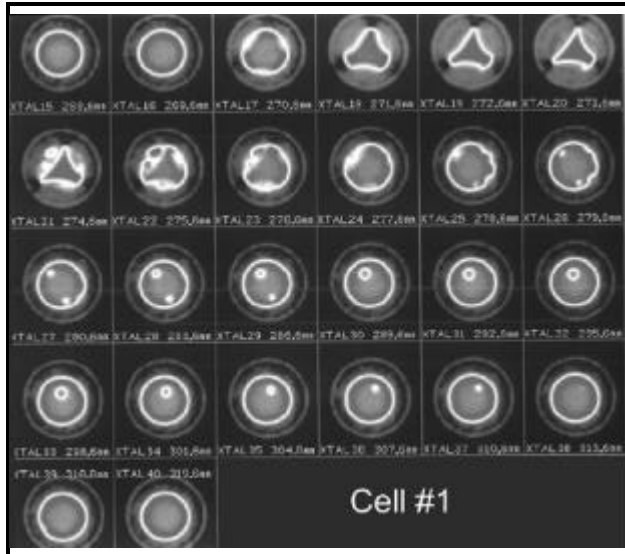


**Figure 9**  
Successive CAT, horizontal, slices of Cell #1. The first to freeze end is at upper left. The first thirteen slices were taken at 1 mm steps and the remaining slices at 3 mm steps. Images were made with 420 KV x-rays.

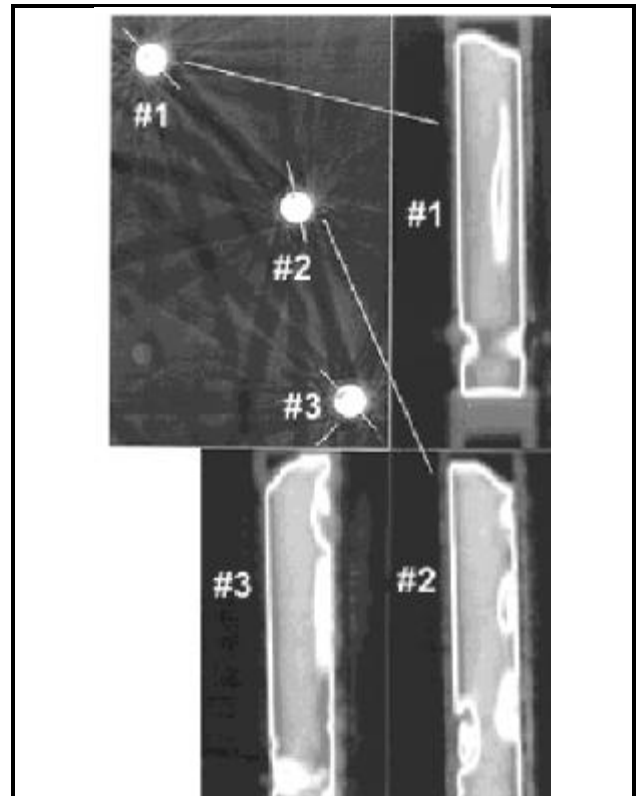


**Figure 8**  
Vertical slices of the three USMP-3 PbSnTe crystals. These scans were made from the integrated results of CAT scans . Each crystal is positioned with the first to freeze end down. The insert at the upper left shows the position of the vertical slice for each crystal.

**Similarities among the three crystals are that the initial formation, in the cold end of each of their respective cells, is a complete solid crystal that completely filled the base of that cell. (This solidarity of structure in the base did not hold upon microscopic examination. This topic will be discussed more fully in a later section.) After the formation of the base section, which is longer than the anomalous compositional distribution due to recalescence, each crystal then necked**

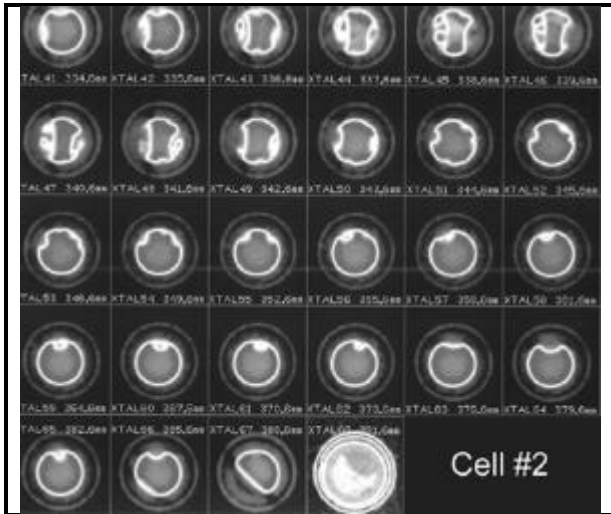


**Figure 10**

Successive CAT, horizontal, slices of Cell #2. The first to freeze end is at upper left. The first thirteen slices were taken at 1 mm steps and the remaining slices at 3 mm steps. Images were made with 420 KV x-rays. The first scan was taken approximately 8 mm above the base of the crystal hence it shows the beginning of the void formation.

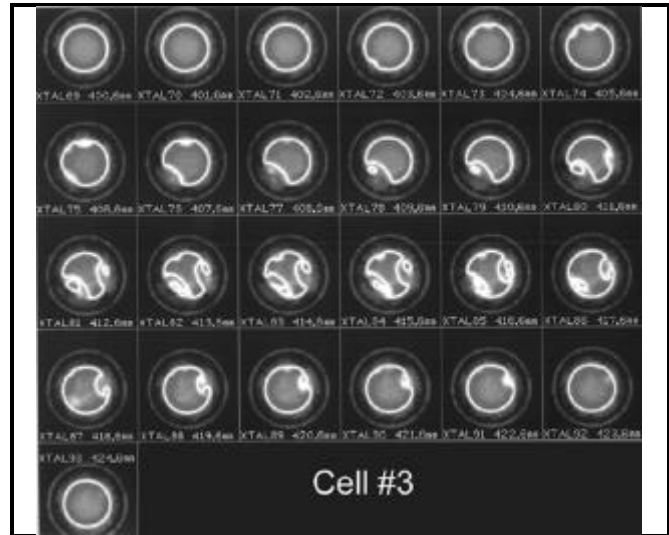


**Figure 11**

Successive CAT, horizontal, slices of Cell #3. The first to freeze end is at upper left. The first twenty six slices were taken at 1 mm steps and the remaining slices at 3 mm steps. Images were made with 420 KV x-rays.

down almost to the point of discontinuity. The channels and cavities emanate from the upper (terms such as base and upper, of course, have their etymology in references to Earth gravity; here they are merely convenient terms to refer to positions relative to the coldest part of each experimental growth cell) ends of the voids that formed the necked down region. Finally, the last to freeze ends of the crystals become solid again.

The primary difference in x-ray appearance is the way a double set of cavities formed in cell #1 as opposed to the surface channels in the other two crystals.

These results were totally unexpected. Large pores or voids have been found in other space grown crystals<sup>19,20</sup>, but no large pores or other voids were found in the PbSnTe crystal grown on the 1985 STS 61A mission, and although Kinoshita<sup>21</sup> reported some porosity, his photographs showed monolithic crystals compared to these.

### Sample Composition

The primary objective of this flight experiment was to examine the effect of the direction of the microgravity vector on the convective mixing of the liquid during directional solidification. The measurable physical parameter that is the most

sensitive monitor of mixing in the liquid is the compositional profile in the solidified crystal. The difference in the analytical solutions for the profiles for both fully mixed and mixing via diffusion alone is shown in figure 12.

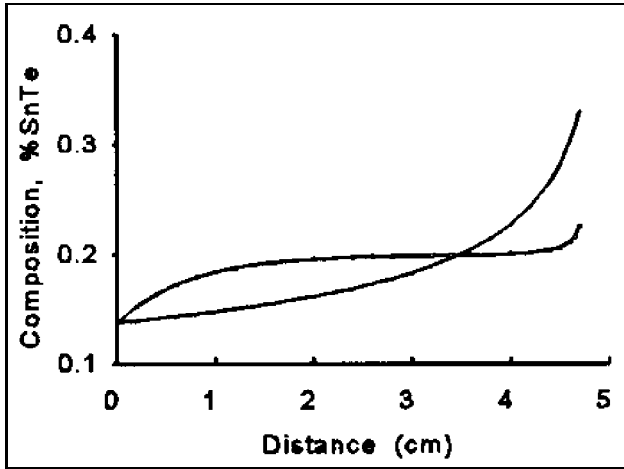


**Figure 12**

Graphs of the one dimensional analytical solutions for the profiles for both fully mixed and mixing via diffusion only during the directional solidification of PbSnTe.

Figures 13 to 15 are axial compositional profiles for cells #1 to 3 respectively. Each cell shows evidence of considerable mixing. With one minor exception, the free drift period already discussed, the Space Shuttle performed the pre-determined maneuvers for the growth periods as required, but the presence of voids creates the condition for surface driven (Marangoni) convection.<sup>22</sup> The problem now becomes that of separating Marangoni convection from density driven convection.

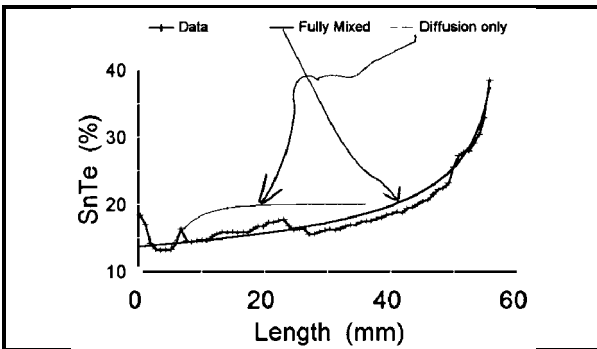


**Figure 13**

Axial composition scan of cell #1. The data scan was made 2 mm from the center line. Also shown are the analytical curves for a totally mixed sample and the start of one grown with diffusion mixing only. The anticipated composition spike of SnTe shows at the recalescence area at the left side of the plot, then the data flattens for what may be growth during thermal stabilization after the release of the latent heat. At 5 mm of growth the composition shows signs of trying to go to diffusion controlled growth. At approximately 25 mm of growth the curve closely approximates the fully mixed case.

Figure 13 shows the axial compositional distribution of cell #1. The anticipated spike of SnTe shows

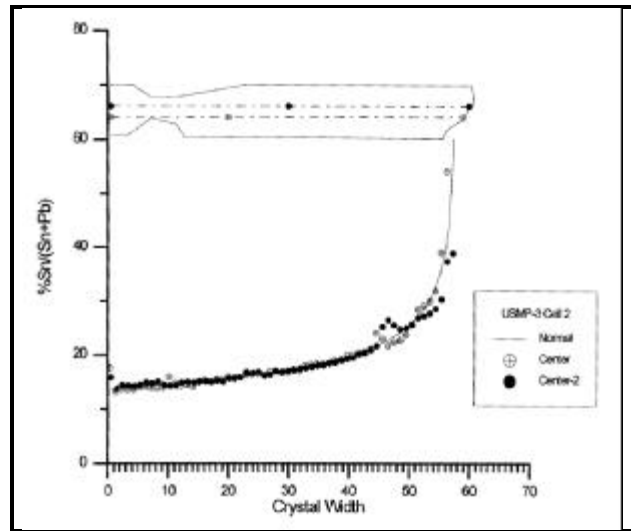


**Figure 14**

Axial compositional profile of the crystal in cell #2, the nominally hot on bottom orientation, follows the completely mixed curve for the first 45 mm of growth and then exhibits deviations that are, as yet, unexplained.

the recalescence area at the left side of the plot, then the data flattens for what may be growth during thermal stabilization after the release of the latent heat. At 5 mm of growth, approximately the length of the produced seed after the solutal diffusion time, the composition shows signs of trying to go to diffusion growth but not making it. At approximately 25 mm of growth the curve closely approximates the fully mixed case. The following deserves further study, but the melt-solid interface would have been 25 mm from the base of cell #1 at approximately MET 08/06/30, the time of the Shuttle free drift which would have essentially turned the AADSF on its side for a few minutes.

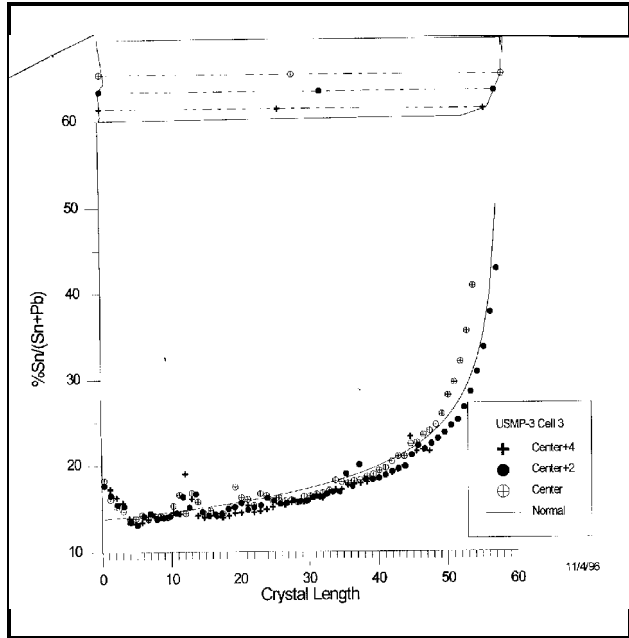


**Figure 15**  
Axial compositional profile of the crystal grown in cell #3. This crystal shows similar deviations from totally mixed as the crystal in cell #2 but over a longer section.

After recalescence the axial compositional profile of the crystal in cell #2, the nominally hot on bottom orientation, follows the completely mixed curve for the first 45 mm of growth and then exhibits deviations (see figure 14) that are, as yet, unexplained. Similar deviations occur in the axial compositional profile of the crystal grown in cell #3, but over a longer section (see figure 15). As yet no acceleration perturbations have been related to these compositional variations. These crystals will be examined to try to correlate these compositional deviations with crystalline microstructure and the defect formation.

### Microporosity

Figures 16 to 18 are photomicrographs of the first to freeze regions of cells #1 to 3 respectively. The first to freeze regions of the crystals grown in cells #1 and 3 clearly

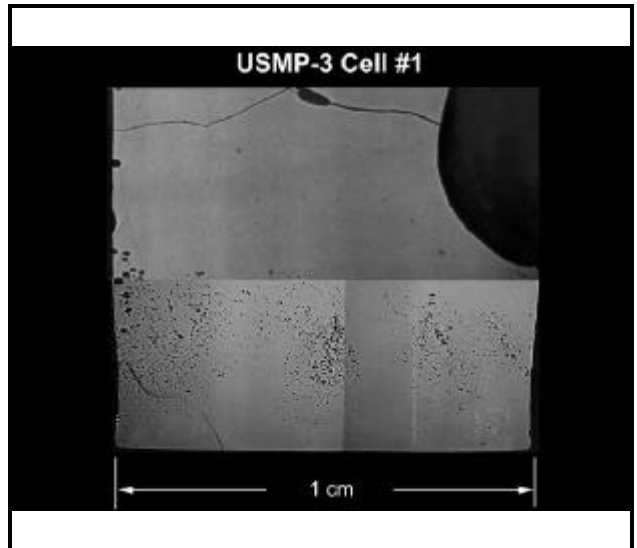


**Figure 16**  
Photomicrograph of the first to freeze region of cells #1. The first to freeze region clearly shows random patterns of sub millimeter pores which were not visible on the CAT scans.

show random patterns of sub millimeter pores which were not visible on the CAT scans. A few pores were seen at the very base of the crystal from cell #2, but the defects are not clearly visible in the attached figure. The volume of the pores in cells #1 and 3 were estimated using a retinex<sup>23</sup> technique to be approximately 4% of total in the base region. This value is the same as the volume reduction upon the phase change from liquid to solid state.

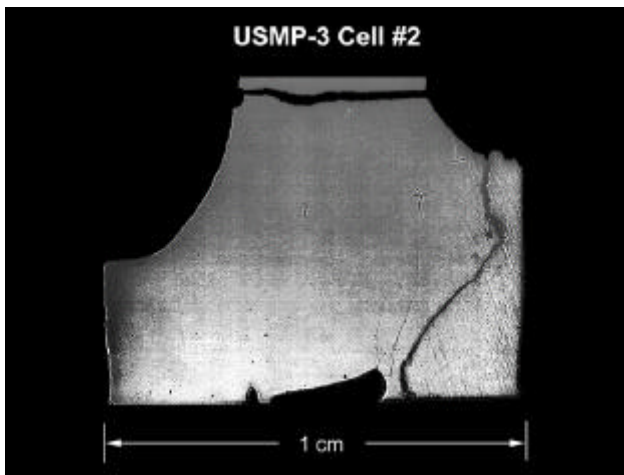


**Figure 17**  
A few pores were seen at the very base of the crystal from cell #2, but the defects are not clearly visible in the photograph.

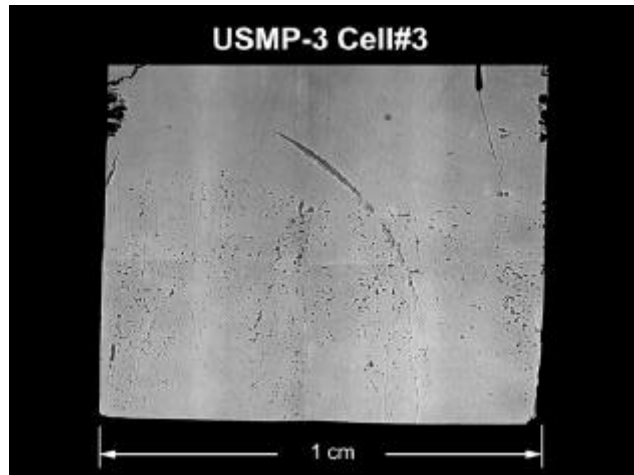


**Figure 18**  
Photomicrograph of the first to freeze region of cell #3. The first to freeze region clearly shows random patterns of sub millimeter pores which were not visible on the CAT scans.

## Summary

This paper is a work in progress for we are far from finishing the analysis of these fascinating and tantalizing samples. We started the flight experiment to determine the small, but predictable, differences in convective mixing due to the alignment of the acceleration vector. We are still trying to extract data on that topic, but such information is buried in the myriad observations of the large pore, void, and channel formations.

We have been able to show a few things within this time frame that are useful to the microgravity materials science community, and we believe that we will deliver a complete story when we complete the evaluation and analysis of the USMP-3 experiment especially when we couple the results with the upcoming USMP-4 crystal growth experiments and the experiments of others in this area.

## **Acknowledgments**

**Many thanks to the many people who made this exciting work possible. To acknowledge everyone who contributed to the years of effort that went into this work would exceed the page limit of this paper. The Investigators are truly humbled by the effort, dedication, sacrifice, and brilliance offered by so many program, project, and support staff that make these esoteric space projects possible. They are the people who do all of the work while we get the glory. Thank you.**

**A precious few must be mentioned by name which in no way detracts from all the rest. We offer special thanks to Bob Rhome who guided the program and encouraged us to stay with it during internal reorganizations; Mike Wargo who shepherded the science and kept us on our toes; Roger Crouch, the sparkplug so vital to us in the earlier days; Fred Reeves, Jim Sledd, and Linda Jeter who kept nuts, bolts, and schedules together; Kent Pendergrass and Wayne Gandy who helped us learn what the furnace could do; Sandor (Alex) Lehoczky, Don Gillies, Peter Curreri, and Sherwood Anderson who guided us to flight; Bob Berry, Dick Simchick, Ned Baker, Glenn Woodell, and Jim Wells who have done so much for us at Langley; and Peter Engel at KSC for his expertise with the CAT unit. To one and all of them I say a very sincere and heartfelt, "Thank you."**

## References

1. T.C. Harman; "Control and Imperfections in Crystals of PbSnTe, PbSnSe and PbSSe"; J.Nonmetals 1 (1973) p 183.
2. S.G. Parker and R.W. Johnson; "preparation and Properties of PbSnTe"; in Preparation and Properties of Solid State Materials vol 6, Ed. W.R. Wilcox, Marcel Dekker, Inc., New York 1981, p 1.
3. S.R. Coriell, M.R. Cordes, W.J. Boettinger and R.F. Sekerka; "Convective and Interfacial Instabilities During Unidirectional Solidification of a Binary Alloy"; J Crystal Growth, vol 49 (1980) p 13.
4. J.H. Hurst, "Electrochemical Visualization of Convection in Liquid Metals", PhD. Dissertation, The University of Florida, Chemical Engineering, (1990).
5. B. Sears, R. Narayanan, T.J. Anderson and A.L. Fripp, "Convection of Tin in a Bridgman System I. Flow Characterization by Effective Diffusivity Measurements"; J. Crystal Growth, vol 125 (1992) p 404.
6. B. Sears, A.L. Fripp, W.J. Debnam, G.A. Woodell, T.J. Anderson and R. Narayanan, "Convection of Tin in a Bridgman System II. An Electrochemical Method for Detecting Flow Regimes"; J. Crystal Growth, vol 125 (1992) p 415.
7. B. Sears, T.J. Anderson, R. Narayanan and A.L. Fripp, "The Detection of Solutal Convection During Electrochemical Measurement of the Oxygen Diffusivity in Liquid Tin"; Metallurgical Transactions B, vol 24B (1993) p 91.
8. F.M. Carlson, A.L. Fripp, and R.K. Crouch; "Thermal Convection During Bridgman Crystal Growth", J. Crystal Growth, 1984, vol 68, p. 747.
9. S. Patankar; " Numerical Heat Transfer and Fluid Flow", Taylor and Francis, Bristol, PA 1980
10. J.J. Favier; "Recent Advances in Bridgman Growth Modelling and Fluid Flow"; J Crystal Growth vol 99 (1990) p 18.
11. W.A. Tiller, K.A. Jackson, J.W. Rutter and B. Chalmers; "The Redistribution of Solute Atoms During the Solidification of Metals"; Acta Met. 1 (1953) p 428.
12. B.P. Matisak, A.X. Zhao, R. Narayanan, and A. Fripp; The Microgravity Environment: its Prediction, Measurement, and Importance to Materials Processing; Presented at The Tenth American Conference on Crystal Growth, August 4-9, 1996, Vail, CO and accepted for publication in the Journal of Crystal Growth
13. A.L. Fripp, R.K. Crouch, W.J. Debnam, I.O. Clark, and J.B. Wagner; "Effects of Supercooling in the Initial Solidification of PbTe-SnTe Solid Solutions;" J. Crystal Growth vol 73 (1985) p304.
14. R.C. Blanchard, M.K. Hendrix, J.C. Fox, D.J. Thomas, and J.Y. Nicholson; "Orbital Acceleration Research Experiment;" J. Spacecraft and Rockets vol 24 (1987) p504.
15. J.I.D. Alexander and C.A. Lundquist; "Motions in Fluids Caused by Microgravitational Acceleration and Their Modification by Relative Rotation;" AIAA 25th Aerospace Sciences Meeting, January 12-15, 1987, Reno, NV, paper AIAA-87-0312.

16. B.P. Matisak, M.J.B. Rogers, and J.I.D. Alexander; "Analysis of the Passive Accelerometer System (PAS) Measurements During USML-1;" AIAA 32nd Aerospace Sciences Meeting, January 10-13, 1994, Reno, NV. paper AIAA-94-0434.
17. R. DeLombard; "Compendium of Information for Interpreting the Microgravity Environment of the Orbiter Spacecraft;" NASA Technical Memorandum 107032, August 1996, NASA Lewis Research Center, Cleveland, OH.
18. B.P. Matisak, "Update to USMP-3/STS-75 AADSF Attitude Design Study"; #410RPT0736, Teledyne Brown Engineering, Huntsville, AL, August 31, 1995.
19. D.H. Matthiesen and J.A. Majewski, "The Study of Dopant Segregation Behavior During the Growth of GaAs in Microgravity"; NASA Conference Publication 3272, vol. 1, p 223, May 1994; Joint Launch + One Year Review of USML-1 and USMP-1 with the Microgravity Measurement Group
20. J.B. Andrews, L.J. Hayes, Y. Arikawa, and S.R. Coriell, "Microgravity Solidification of Al-In Alloys"; 35th Aerospace Sciences Meeting, AIAA, Reno, NV, January 6-10, 1997.
21. K. Kinoshita and T. Yamada; "PbSnTe Crystal Growth in Space," J Crystal Growth, vol 147 (1995) p 91.
22. R.J. Naumann, "Marangoni Convection Around Voids in Bridgman Growth"; J. Crystal Growth, vol 154, (1995) p 156.
23. D.J. Jobson, Z. Rahman, and G.A. Woodell; "Properties and Performance of a Center/Surround Retinex," IEEE Transactions on Image Processing, vol 6, (1997) p 451.